AGU PUBLICATIONS

Radio Science

RESEARCH ARTICLE
10.1002/2015RS005842

A directional HF noise model: Calibration and validation in the Australian region

L. H. Pederick[1] and M. A. Cervera[1,2]

[1]Defence Science and Technology Group, Edinburgh, South Australia, Australia, [2]School of Physical Sciences, The University of Adelaide, Adelaide, Australia

Key Points:
- We have developed a model for radio noise at HF
- Can model diurnal, seasonal, and geographic variations
- Model has been calibrated and validated using data from multiple JORN sites

Correspondence to:
L. H. Pederick,
lenard.pederick@dsto.defence.gov.au

Citation:
Pederick, L. H., and M. A. Cervera (2016), A directional HF noise model: Calibration and validation in the Australian region, *Radio Sci.*, *51*, 25–39, doi:10.1002/2015RS005842.

Received 26 OCT 2015
Accepted 8 DEC 2015
Accepted article online 14 DEC 2015
Published online 23 JAN 2016
Corrected 15 FEB 2016

This article was corrected on 15 FEB 2016. See the end of the full text for details.

Abstract The performance of systems using HF (high frequency) radio waves, such as over-the-horizon radars, is strongly dependent on the external noise environment. However, this environment has complex behavior and is known to vary with location, time, season, sunspot number, and radio frequency. It is also highly anisotropic, with the directional variation of noise being very important for the design and development of next generation over-the-horizon radar. By combining global maps of lightning occurrence, raytracing propagation, a model background ionosphere and ionospheric absorption, the behavior of noise at HF may be modeled. This article outlines the principles, techniques, and current progress of the model and calibrates it against a 5 year data set of background noise measurements. The calibrated model is then compared with data at a second site.

1. Introduction

The performance of high frequency radar systems (such as over-the-horizon radar) is highly dependent on the external noise environment. This environment is variable and depends on the frequency, geographic location, the time of day, the season, and sunspot number. The noise is also highly anisotropic, with the directional distribution being an important consideration for the design of next generation radars with 2-D receive arrays.

Radio noise at high frequency (HF) has been a subject of much research over many decades. In the 1930s, atmospheric measurements at high or middle frequency bands were started in many countries and considerable knowledge was gained about the variations of atmospheric noise. However, the methods of measurements were not standardized, making intercomparisons of the results difficult [*Kotaki*, 1984]. In the 1950s, as demand increased for improved quality of telecommunications and basic data were required for the frequency allocation of broadcast and communication links, the eighth Plenary Assembly of the CCIR (International Radio Consultative Committee) adopted a plan for establishing networks to observe atmospheric radio noise. In 1963, based on the data collected, CCIR presented a report of the "World Distribution and Characteristics of Atmospheric Radio Noise" [*International Radio Consultative Committee*, 1964].

CCIR and its successor organization the International Telecommunications Union (ITU) have continued maintaining and updating its model of external noise at HF. The most recent revision of this model is given in ITU-R P.372-11 [*International Telecommunication Union*, 2013]; however, this model is known to have major differences from noise measurements taken in the Southern Hemisphere [*Northey and Whitham*, 2000].

There have been many other efforts to measure and model the external noise environment at HF, particularly its temporal characteristics [*Shinde and Gupta*, 1974; *Lemmon*, 1991, 2001; *Giesbrecht et al.*, 2006]. Kotaki developed a model based on the global distribution of thunderstorm activity [*Kotaki*, 1984], which was improved using a more accurate propagation model by *Coleman* [2002]. There have also been several noise measurement campaigns conducted in locations relevant to U.S. and Australian over-the-horizon radar (OTHR) [*Ward and Golley*, 1991; *Rodriguez*, 1997; *Northey and Whitham*, 2000].

The design of next generation OTHR systems often includes two-dimensional receive arrays. In order to correctly model the performance of these arrays and ensure that the extra gain afforded by these designs leads to increased sensitivity of the whole radar system, it is important to have an accurate model for the external noise environment, particularly its directional distribution.

The System for the Prediction of the Interference and Noise Environment (SPINE) noise model described in this paper is based on a theoretical framework developed by *Coleman* [2002], who combined global maps of

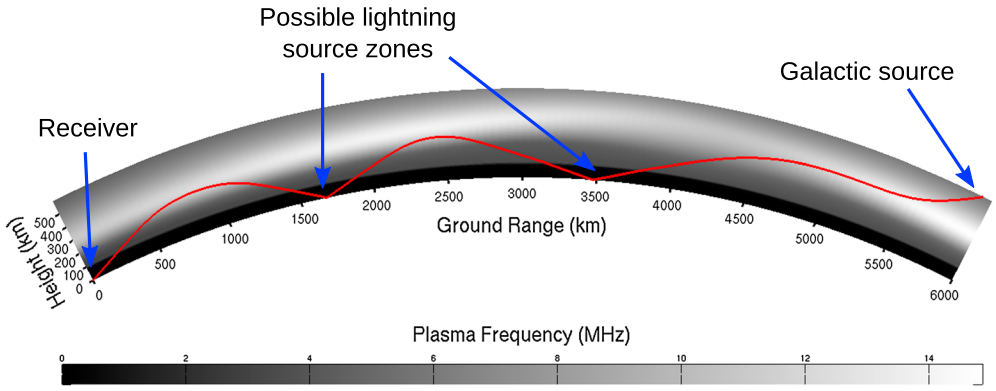

Figure 1. An example of a raytrace in a particular direction, showing noise coming from two different lightning sources and a galactic source. In this example the receiver is at 23.5°S, 133.7°E, with the ray traced at a bearing of 324.7°at 22°above the horizon. The frequency is 22 MHz and the ionosphere is from IRI, calculated for 15 March 2001 07:00 UTC at an R_{12} of 100.

lightning occurrence with raytracing propagation calculations to form a direction-sensitive model of radio noise. While the theory behind the noise model remains, we have built upon the Coleman model in several areas: (1) calibration using noise data from the Jindalee Operational Radar Network (JORN) Frequency Management System (FMS) at Longreach; (2) validation of the model against noise data from the JORN FMS at Laverton, which is 2160 km away from Longreach; (3) a more accurate absorption model, which is an important contribution to the noise model particularly at lower frequencies; (4) updated lightning strike models; and (5) a directional galactic noise model. We have also explored the use of three-dimensional numerical raytracing to model the noise on the *O* and *X* polarization modes separately.

Calibration and validation were done against a background noise data set from the JORN FMS, from three sites across Australia. This is a comprehensive and unique data set of synoptic noise measurements covering a whole solar cycle. These data are described in section 4 along with the calibration and validation procedure.

Preliminary results from this model have already been used in the design of new receiving arrays for over-the-horizon radar [*Frazer et al.*, 2015], as a realistic external noise distribution is a vital component of the design strategy for this array.

This article will report only on the noise component of SPINE; the interference component is reported in L. H. Pederick and M. A. Cervera (Modeling the interference environment in the HF band, submitted to *Radio Science*, 2015).

2. Noise Model

At HF, natural external noise originates chiefly from two sources. The major source is lightning strikes, which can be separated into two components: a local component (which propagates to the receiver via line of sight or ground waves, for example, when a thunderstorm is within 100 km of the receive system) and an ionospheric component (which propagates to the receiver via the ionosphere). The ionospheric component is the combination of energy from the many lightning strikes across the globe (approximately 170,000 per hour, across the whole world, as calculated from *Cecil et al.* [2014], varying with season and time of day) and results in a consistent "drizzle" of noise. The other natural source is galactic noise, which originates from outside the Earth environment and propagates through the ionosphere. As it requires transionospheric propagation this noise is only present at higher frequencies or high elevation angles; radio waves at lower frequencies and low elevation angles cannot penetrate the ionosphere.

For a given azimuth, elevation, frequency, and ionospheric condition, the locations on the globe that could contribute to the environmental noise can be determined using raytracing. An example is shown in Figure 1, showing a direction in which there are two sources of lightning noise and a galactic noise source (the ray exiting the ionosphere indicates that galactic noise contributes). Once these locations are determined, the noise density per unit solid angle *N* can be calculated as:

$$N(\theta,\phi) = \sum_i N_i(\theta,\phi), \tag{1}$$

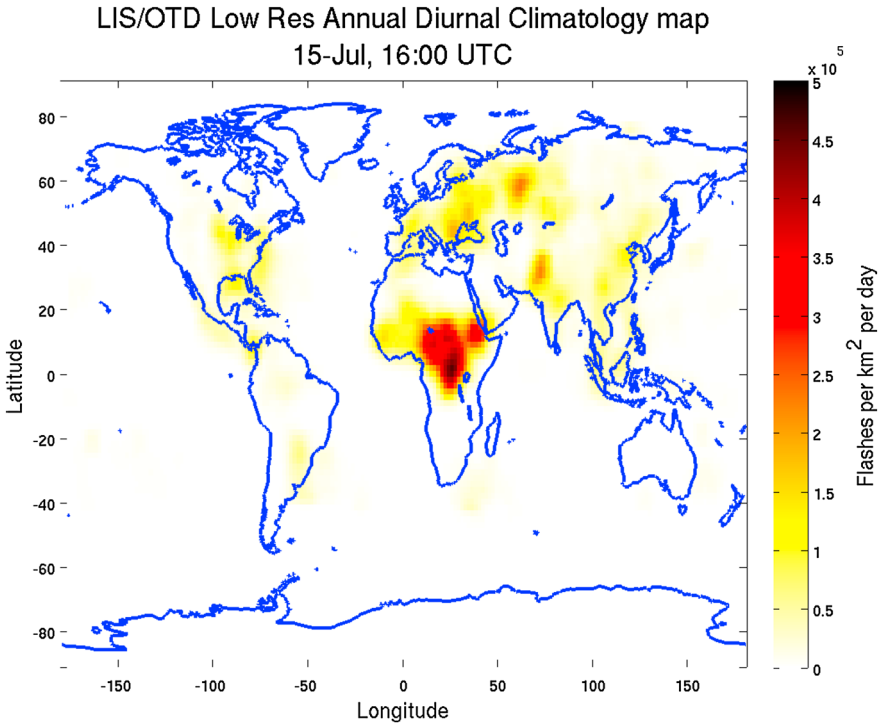

Figure 2. The lightning strike rate from the LIS/OTD Annual Diurnal Climatological lightning model, for 15 July at 16:00 UTC.

where

$$N_i(\theta,\phi) = \begin{cases} \left(\frac{\lambda}{4\pi}\right)^2 \frac{W(f)S_i}{L_i \sin(\varphi_i)} & \text{for lightning source} \\ \left(\frac{\lambda}{4\pi}\right)^2 \frac{G(f,\theta,\phi)}{L_i} & \text{for galactic source,} \end{cases} \quad (2)$$

and θ and ϕ are azimuth and elevation, λ is the radio wavelength, f is the radio frequency, W is the radiated energy density of a lightning strike, S_i is the strike rate at the start point of the propagation path, G is the galactic noise density in a particular direction, φ_i is the elevation at which the noise left the thunder storm, and L_i is the loss due to both ionospheric absorption along the propagation path and ground reflections. The summation is carried out over each reflection from the ground, i.e., $i = 1, 2, 3 \ldots$ with each successive term representing the contribution from lightning strikes that are one additional ionospheric hop further from the receiver (in practice the sum is terminated after a small number of reflections, usually 3 to 5, depending on the precision desired).

The form of the ith term in the sum, N_i, depends on whether the propagation for the ith hop in a given direction (θ, ϕ) originated from the Earth, indicating the source is lightning noise, or if it propagated transionospherically, which means the source is galactic.

It should be noted that the distance to the source of the noise does not appear in the formula for N, as the lightning strikes are treated as an area source rather than a point source, so an increase in distance will be canceled out by a corresponding increase in the total area of the noise source seen by the receiver in a given area of solid angle. Similarly, any focussing or defocussing effects caused by the ionospheric propagation will not affect the noise density.

2.1. Lightning Strike Noise

The lightning strike rate S_i is approximated using NASA's LIS/OTD Low Resolution Annual Diurnal Climatological lightning model [*Cecil et al.*, 2014]. This model is derived from over 16 years of data from two satellite-borne sensors, the Optical Transient Detector (OTD) on the Microlab-1 satellite and the Lightning Imaging Sensor (LIS) on the Tropical Rainfall Measuring Mission. It provides lightning strike rates (in flashes km^{-2} day^{-1}) for any given day of the year, time of day, and geographic location. An example of this model's output is shown in Figure 2.

In the LIS/OTD model, lightning strikes are more often observed over land masses, especially those in the tropics; there is much less lightning observed over the oceans and almost none over the polar regions. Lightning is also most common in the early afternoon and in the summer months.

Converting the lightning strike rate given by the LIS/OTD model into a radio noise power value requires knowledge of W, the radiated power per lightning strike. This is discussed further in section 4.

2.2. Galactic Noise

The galactic noise G is approximated using a model adapted from de Oliveira-Costa et al.'s model of diffuse galactic radio emission [*de Oliveira-Costa et al.*, 2008]. This is a global sky model derived from all publicly available total power large-area radio surveys which can return a predicted all-sky map at any frequency from 10 MHz to 100 GHz. SPINE uses the sky map calculated by de Oliveira-Costa et al.'s model at 20 MHz, with the power scaled in the same manner as the galactic noise component of ITU-R P.372 [*International Telecommunication Union*, 2013] to give the noise power at other frequencies:

$$G(f,\theta,\phi) = G_{20}(\theta,\phi) - 23\log_{10}\frac{f}{20}, \tag{3}$$

where θ and ϕ are azimuth and elevation, G_{20} is the sky map calculated at 20 MHz in dBW Hz^{-1} sr^{-1}, and f is the radio frequency in MHz.

3. Propagation

The raytracing to determine the location of relevant noise sources is performed using the PHaRLAP numerical raytracing software [*Cervera and Harris*, 2014]. Two-dimensional numerical raytracing (2-D NRT) over a spherical Earth is used, as opposed to three-dimensional NRT, for simplicity and speed; due to the large geographical extent of the noise sources (i.e., thunderstorms), the differences caused by magneto-ionospheric splitting, ionospheric tilts or the Earth's oblateness are small enough to ignore — see section 6.

The electron density in the ionosphere was modeled using the International Reference Ionosphere [*Bilitza et al.*, 2011], the de facto international standard for the climatological specification of ionospheric parameters. International Reference Ionosphere (IRI) produces monthly median values of ionospheric electron densities and temperatures in the nonauroral ionosphere, and can model diurnal, seasonal, solar cycle, and geographic variations. It should be noted that this model does not account for the effects of sporadic E.

3.1. Absorption Model

The losses due to absorption by the ionosphere are calculated using the SiMIAN absorption model [*Pederick and Cervera*, 2014]. This model integrates the absorption coefficient χ (the imaginary component of the complex refractive index) along a ray path, with the absorption coefficient calculated using the Sen-Wyller formula [*Sen and Wyller*, 1960] and the NRLMSISE-00 atmospheric model [*Picone et al.*, 2002].

This absorption model represents a significant improvement over that used in Coleman's noise model [*Coleman*, 2002] which used a much simpler empirical form given by *Lucas and Haydon* [1966], plus a correction for deviative absorption. Figure 3 shows an example of the differences between the two absorption models. A vertical fan of rays at 13 MHz was traced for a particular set of ionospheric conditions (IRI, for 15 March 2001 07:00 UTC at an R_{12} of 100), with the absorption calculated for each ray using both models. Significant differences between the models can be seen, particularly at elevations around 7°, where the radio propagation changes from being reflected by the E layer (at lower elevations) to the F layer (at higher elevations). In this region the ray is refracted within the layer at a highly oblique angle, close to parallel to the layer; the total distance the ray travels thus becomes large, which should lead to an overall increase in the absorption. This increase in absorption is not seen in the absorption model used by Coleman but is reproduced by SiMIAN. In addition, SiMIAN can be used to calculate the absorption of transionospheric rays, allowing a more accurate prediction of the power density of galactic noise. SiMIAN has other advantages which are described in detail in *Pederick and Cervera* [2014].

The absorption model has a significant effect on the noise density calculated by the model, particularly at lower frequencies during the daytime, where there is more absorption. Consequently, the fidelity of the absorption model is an important consideration for SPINE.

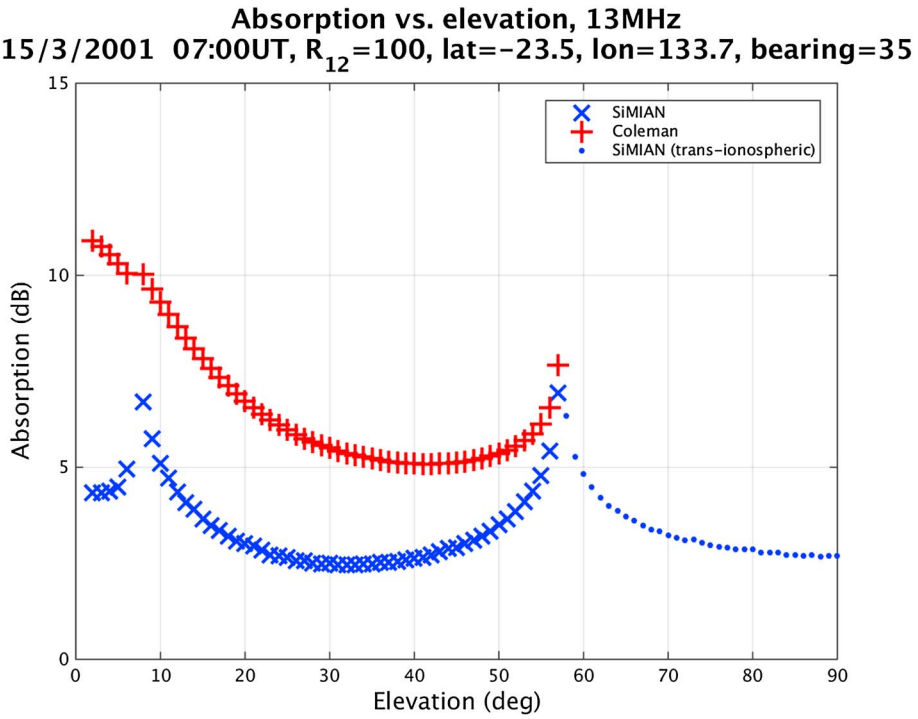

Figure 3. An example showing the difference between the absorption model used in SPINE (SiMIAN) and that used in Coleman's noise model, calculated for a vertical fan of rays.

3.2. Ground Reflection Losses

As in *Coleman's* model [2002], the ground reflection part of the loss L_i is given by

$$L_r = 10\log_{10}\left(\frac{|R_v|^2 + |R_h|^2}{2}\right), \tag{4}$$

where

$$R_v = \frac{n^2\sin\varphi - \left(n^2 - \cos^2\varphi\right)^{\frac{1}{2}}}{n^2\sin\varphi + \left(n^2 - \cos^2\varphi\right)^{\frac{1}{2}}}, \tag{5}$$

$$R_h = \frac{\sin\varphi - \left(n^2 - \cos^2\varphi\right)^{\frac{1}{2}}}{\sin\varphi + \left(n^2 - \cos^2\varphi\right)^{\frac{1}{2}}}, \tag{6}$$

$$n^2 = \varepsilon_r - j(1.8\times10^4)\frac{\sigma}{f}, \tag{7}$$

ε_r is the relative dielectric constant of the Earth surface (using values of 80 for sea and 15 for land), σ is the conductivity of the surface (using 8 S/m for sea and 0.01 S/m for land), f is the propagation frequency, and φ is the elevation at which the ray hits the Earth's surface.

4. Calibration

Within the noise model there are a few parameters which are difficult to determine exactly. The most important is W, the radiated noise power per lightning strike. The mechanism whereby lightning produces HF and VHF radiation is not completely understood [*Cooray*, 2003] and W is difficult to determine theoretically. Instead, W can be determined empirically by comparing the model's output with measured noise data.

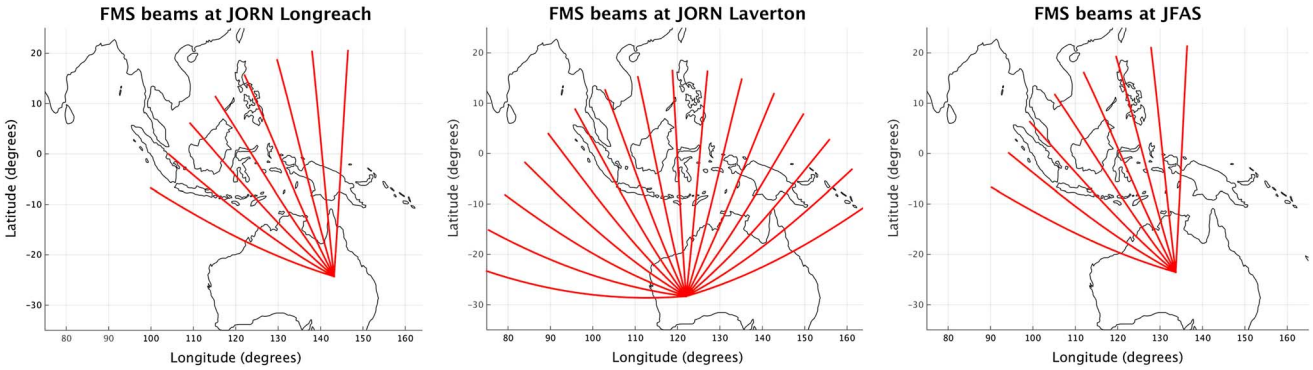

Figure 4. Map depicting the location of each of the JORN radar sites and the direction of each of the FMS beams.

4.1. The JORN Frequency Management System

Calibration of the noise model requires a large database of noise measurements. The data used for calibrating the SPINE noise model were obtained from the Jindalee Operational Radar Network (JORN).

JORN comprises three over-the-horizon radar (OTHR) systems providing wide area surveillance of Australia's northern approaches. The radars are dispersed across Australia, at Longreach in Queensland, Laverton in Western Australia, and Alice Springs in the Northern Territory. To support the operation of the radar, JORN has a Frequency Management System (FMS) which has a number of different sensors, including vertical and oblique

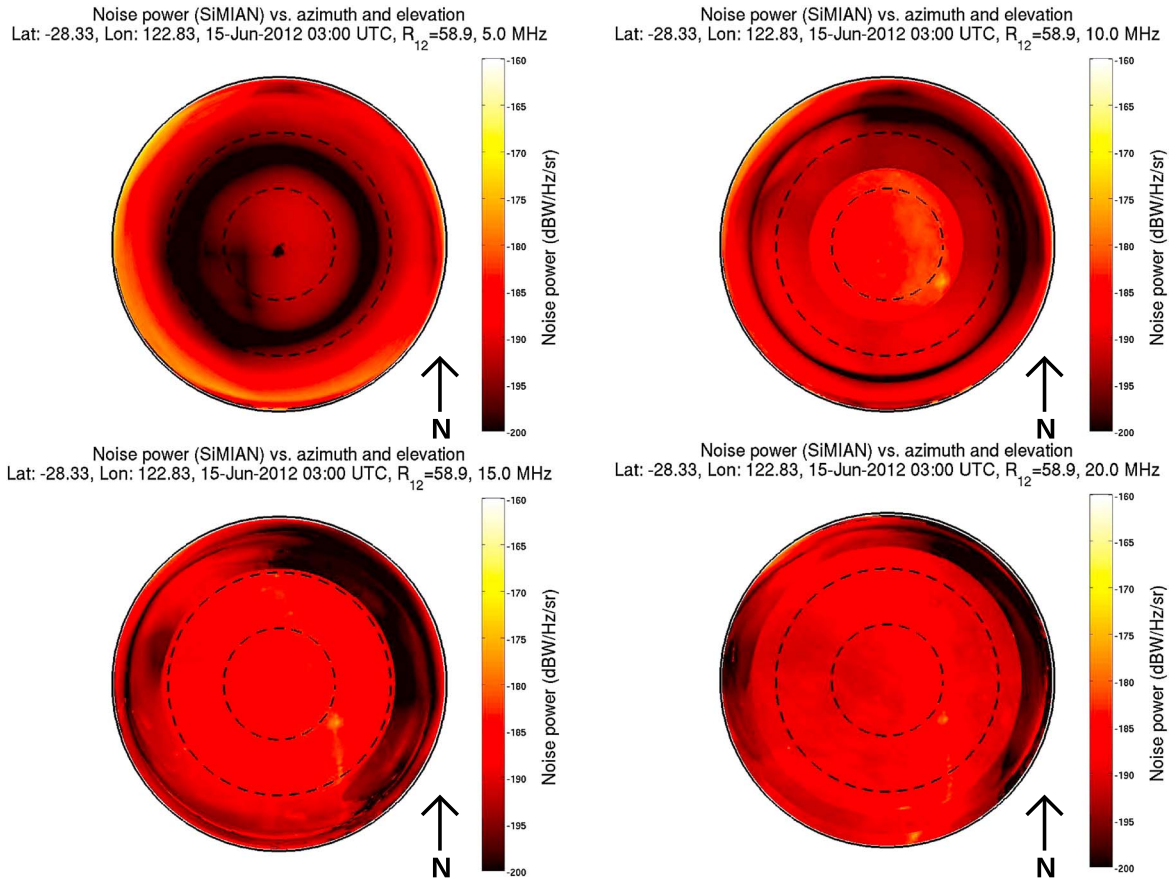

Figure 5. Directional noise densities calculated by SPINE, for frequencies of 5, 10, 15, and 20 MHz during daytime mid solar cycle conditions. The central point of each plot is the zenith, the outer boundary is the horizon and the two dashed circles represent 30° and 60° elevations.

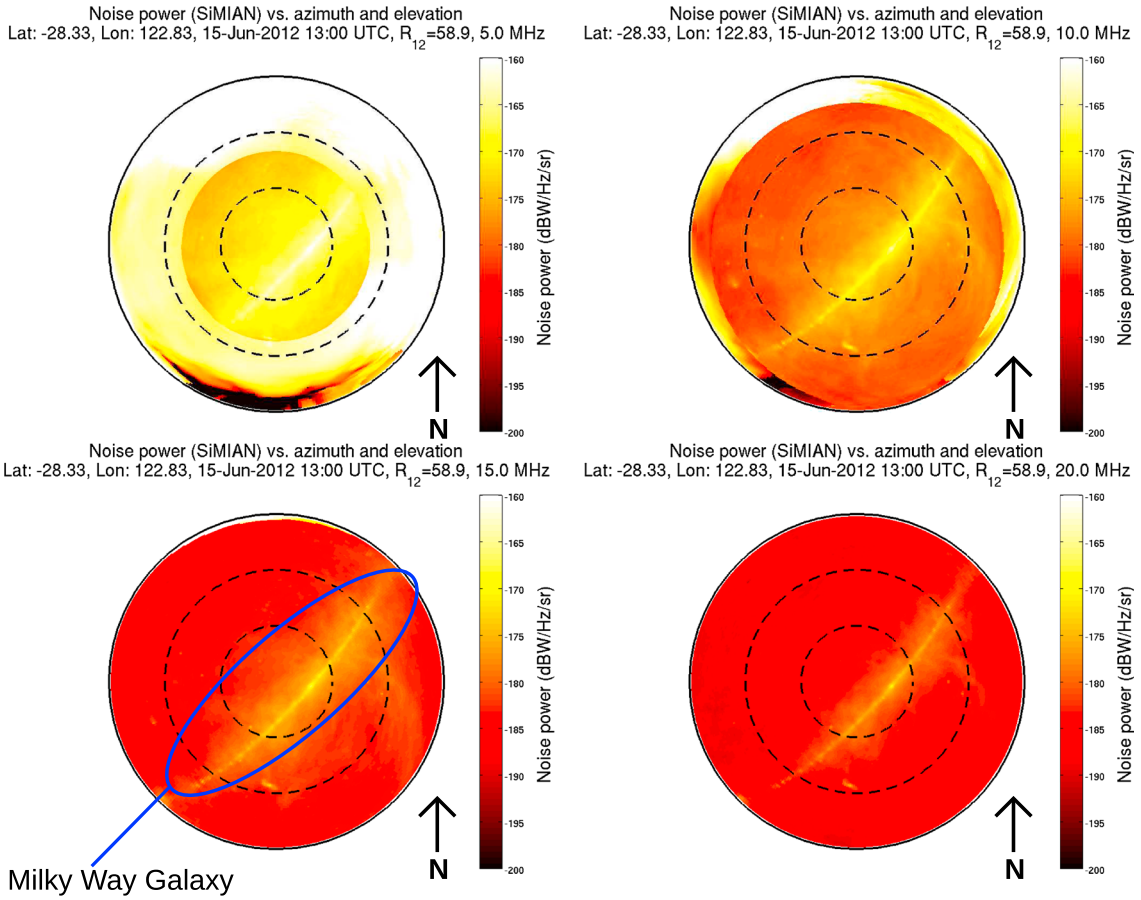

Figure 6. Directional noise densities calculated by SPINE, for frequencies of 5, 10, 15, and 20 MHz during nighttime mid solar cycle conditions. The central point of each plot is the zenith, the outer boundary is the horizon and the two dashed circles represent 30° and 60° elevations.

incidence sounders as well as a backscatter sounder, spectrum monitor, and background noise measurement system at each radar site.

At the Longreach receive site (24.3°S, 143.2°E), the background noise level is measured using a 32 element linear array. Each element is a "doublet," a pair of vertical monopoles in an endfire configuration with a hardware combiner which maximizes the front-to-back-ratio of the antenna system; the 32 doublets are arranged in a broadside array with 6.2 m spacing. From the 32 element array, eight separate beams are formed, covering a 90°arc centered on the radar's boresight (325°, to the northwest); the beams are depicted in Figure 4 (left). The beams farthest to the west are pointed toward Southeast Asia, an area of significant lightning activity and high background noise, whereas the beams farthest to the north are pointed over the Pacific Ocean, which has much less lightning activity and background noise. The data from this system were used to calibrate the model. A similar system is used at the Alice Springs receive site (23.5°S, 133.7°E); this system has a slightly shorter array (28 elements). This receive site and its eight beams are depicted in Figure 4 (right).

The FMS at Laverton (28.3°S, 122.0°E) is similar to the system at the other sites, except that there are two perpendicular 32 element arrays: a west array with a boresight of 325°and an east array with a boresight of 35°(corresponding to the two perpendicular receive arrays, as well as the transmit arrays). The system forms 16 beams covering a 180°arc, including beams pointed at very different noise environments (Indonesia and Malaysia, the Indian Ocean, and the Pacific Ocean); these beams are depicted in Figure 4 (middle).

4.2. Calibration Procedure

SPINE was used to calculate the background noise level at Longreach, across the HF band (5 to 30 MHz) and at 20 min intervals over the entire day, for eight representative months: March, June, September, and December, in 2008 (low solar activity) and in 2012 (high solar activity). The antenna patterns and the power

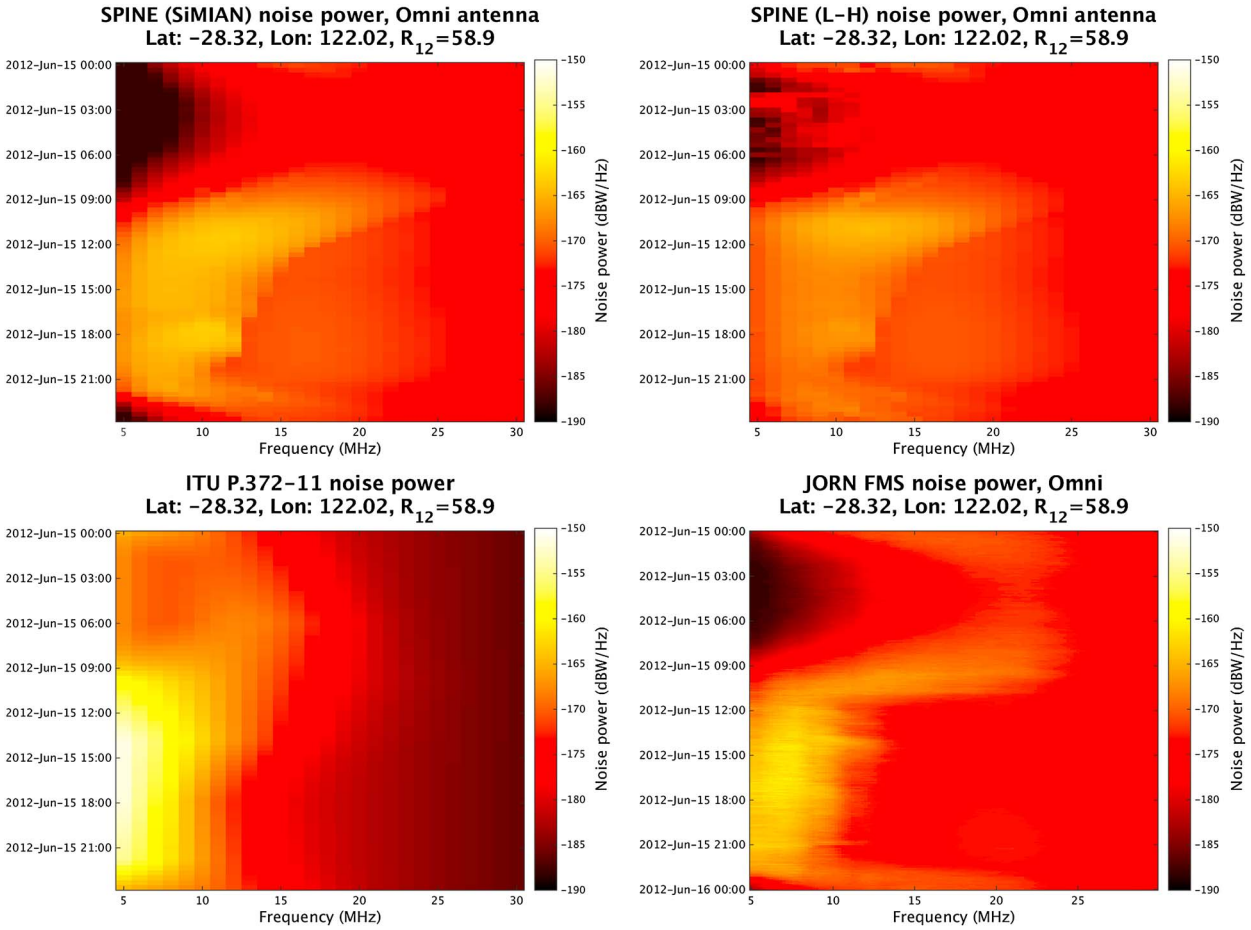

Figure 7. Total background noise seen by a vertical monopole at JORN Laverton, during June 2012, as calculated using different models. Clockwise from top left: SPINE using the SiMIAN absorption model (the default), SPINE using the Lucas and Haydon absorption model (as used in Coleman's work), corresponding monthly median measurements from the JORN FMS and corresponding predictions from the ITU-R P.372 noise model.

loss due to impedance mismatch, for all eight beams formed by the JORN FMS, were modeled using Numerical Electromagnetics Code (NEC) [*Burke*, 1992]. The factor W required to minimize the root-mean-square difference between the model results and the measurements was calculated, assuming that W varies with the logarithm of the frequency, i.e.,

$$W(f) = c_1 \log_{10} f + c_2 \tag{8}$$

where c_1 and c_2 are the logarithmic and constant calibration factors. From this analysis, the values of c_1 and c_2 were −29.9 dB per decade and −243.3 dB, both relative to 1 J sr^{-1} per (flash/km^2). After calibration, the root-mean-square difference between the modeled and the measured data (taken over all of the representative months and all 8 of the FMS beams) was 4.2 dB.

For comparison, if the same measurements are compared against the ITU-R P.372 noise model (including the impedance mismatch from the NEC antenna model), the root-mean-square difference is 4.9 dB.

5. Results

We will now use the calibration constants derived from the JORN FMS measurements at Longreach to calculate the background noise at Laverton. The JORN site at Laverton is 2160 km west of Longreach, at a latitude 4°further south, thus by comparing the calculated noise to measurements from this site we can demonstrate SPINE's ability to model differences in the background noise due to geographic variation.

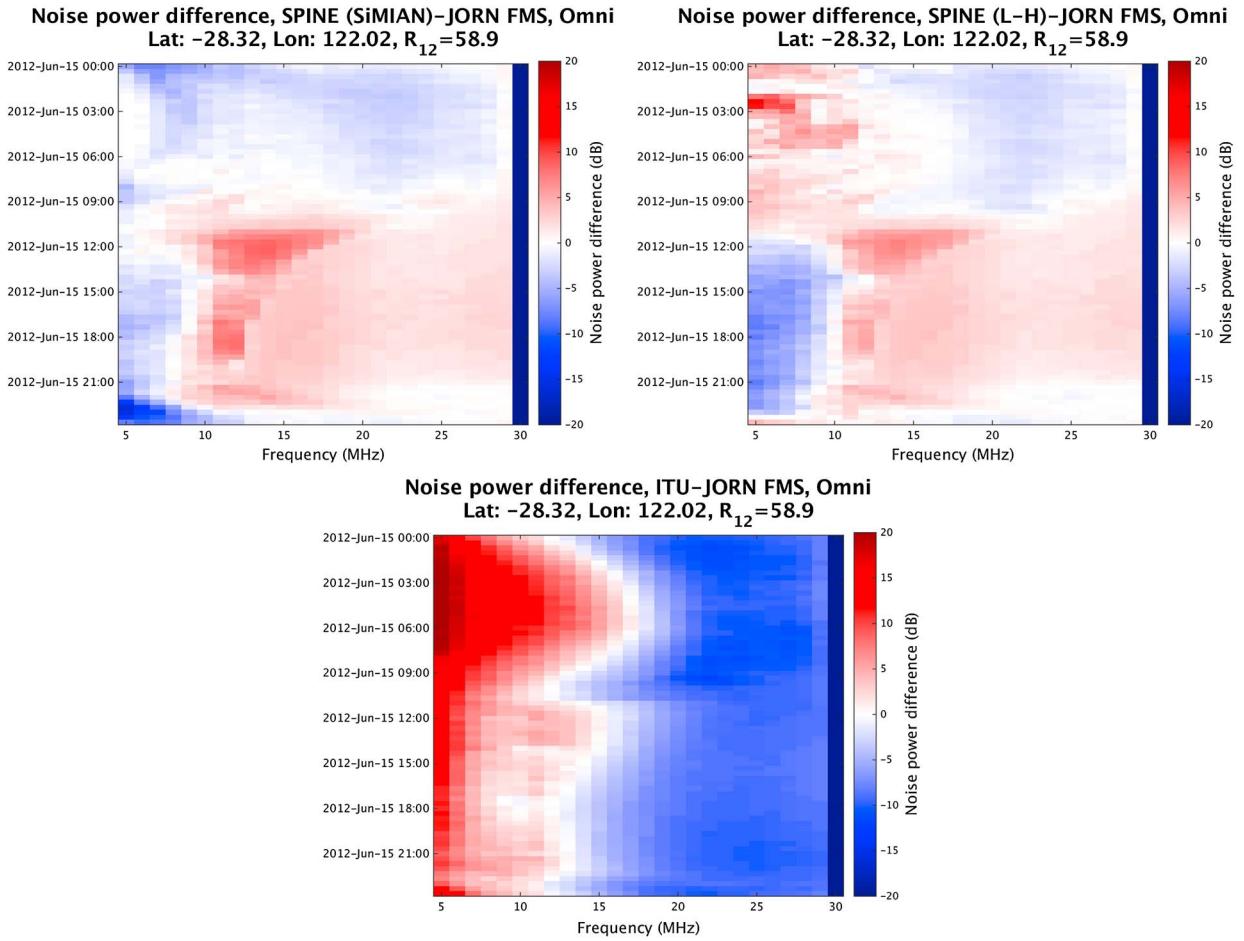

Figure 8. Differences between the various models shown in Figure 7 and the monthly median JORN FMS measurements. Clockwise from top left: difference between SPINE using SiMIAN and JORN FMS noise data set, difference between SPINE using the Lucas and Haydon model and JORN FMS noise data set and difference between ITU-R noise model and JORN FMS noise data set.

5.1. Directional Distribution

Figure 5 shows the directional noise output from SPINE for several frequencies from 5 to 20 MHz, for a receiver at Laverton during June 2012 (R_{12} = 58.9) at 0300 UTC (11:00 local time). Several morphological features generally found in daytime directional noise distributions can be seen. All the plots except 5 MHz show a central area, at high elevations around the zenith, where galactic noise can be seen – note that the position of the galaxy will vary both diurnally and yearly, as the Earth's orientation relative to the stars changes. At lower elevations lightning-generated HF noise propagating to the receiver via the *F* layer can be seen. On two of the plots (10 and 15 MHz), near the horizon, noise propagating via the *E* region can also be seen. Between these distinct regions of propagation, rings of reduced noise power can be seen where the radio waves take a longer path through the ionosphere and have consequently higher absorption. Also, the overall noise level decreases at lower frequencies as the radio waves are absorbed more strongly by the ionosphere.

Figure 6 shows similar output but under nighttime conditions at Laverton (1300 UTC, 21:00 local time). Two main differences from the daytime results can be seen: (1) less lightning noise and more galactic noise can be seen and (2) the amount of absorption due to the *D* region is reduced. Thus, at higher frequencies, there is less noise than during the daytime as most of the noise background is due to the galactic noise (which is weaker than lightning noise), whereas at lower frequencies the noise is greater than that during the daytime due to the decrease in absorption. The directional distribution of the galactic noise is more visible here than in the daytime results, with the central band of the Milky Way galaxy running across the sky from northeast to southwest.

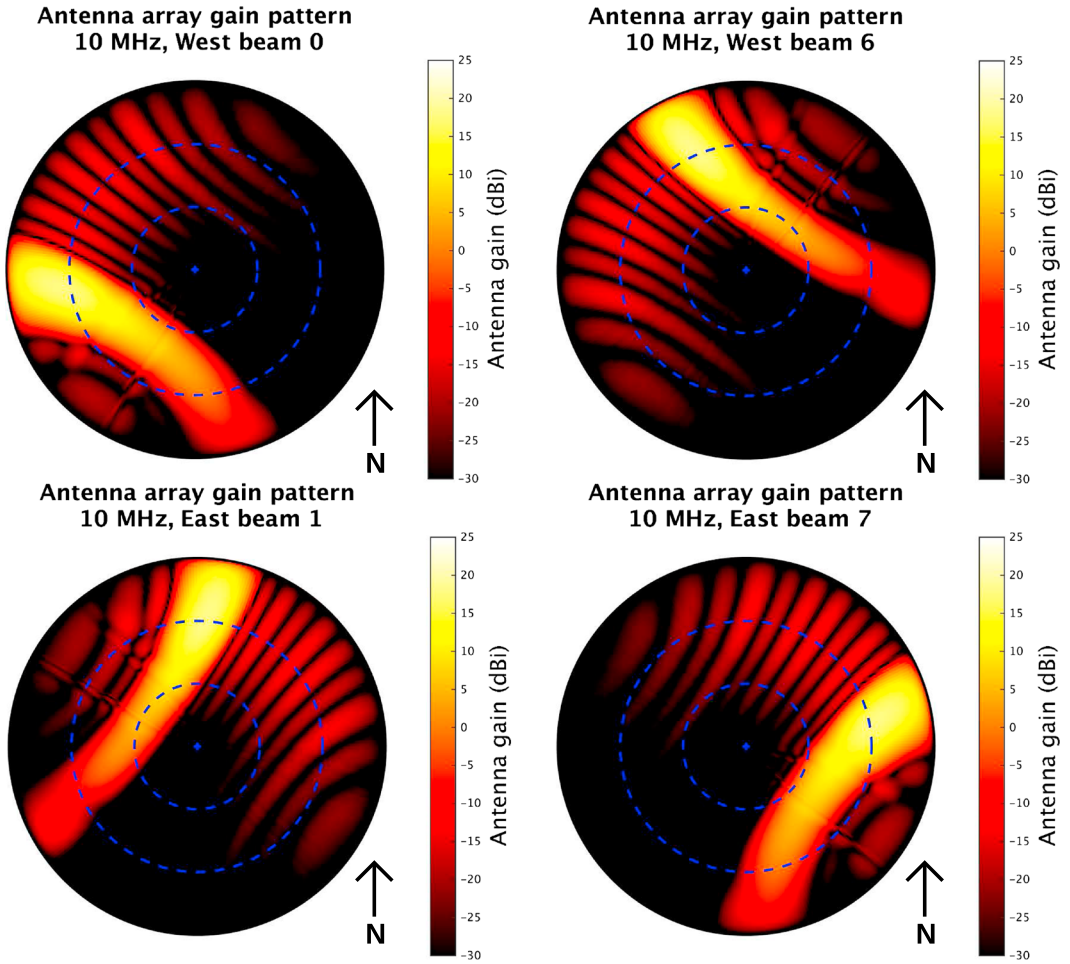

Figure 9. Antenna array gain patterns for the FMS array at JORN Laverton, for four different beams, at 10 MHz, calculated using NEC. The central point of each plot is the zenith, the outer boundary is the horizon and the two dashed circles represent 30° and 60° elevations. True north is at the top of the diagram.

5.2. Diurnal and Frequency Variation

Figures 7 and 8 show the total noise power expected to be received by a vertical monopole as a function of time of day and frequency, from 5 to 30 MHz. Results calculated using several different models are shown. Figure 7 (top row) shows the SPINE results, using two different absorption models (the default SiMIAN absorption model and the *Lucas and Haydon* model [1966] as used in *Coleman's* work [2002]). The bottom left panel shows results from the ITU-R P.372 noise model [*International Telecommunication Union*, 2013] and the bottom right shows the corresponding measurements from the JORN FMS at Laverton, made using the omnidirectional whip antenna.

Figure 8 shows the differences between the three noise models and the JORN FMS noise data set. Both SPINE results match the JORN data more closely than the ITU-R noise, with a smaller overall difference and a better representation of the frequency dependence of the measured background noise level. The two SPINE models differ mainly in the lower frequencies (5 to 10 MHz), with the Lucas and Haydon model giving too much absorption at nighttime and spurious artifacts during the daytime. SPINE using the SiMIAN absorption model matches the JORN data the best out of all three models (having a smaller mean absolute difference than the other two noise models), demonstrating the importance of having an accurate absorption model in accurately estimating the background noise.

5.3. Directional Antenna Array Model Comparison

The differences between SPINE and the ITU-R P.372 noise model are more apparent when SPINE is used to model the background noise seen by a directional antenna array. The ITU-R model does not include

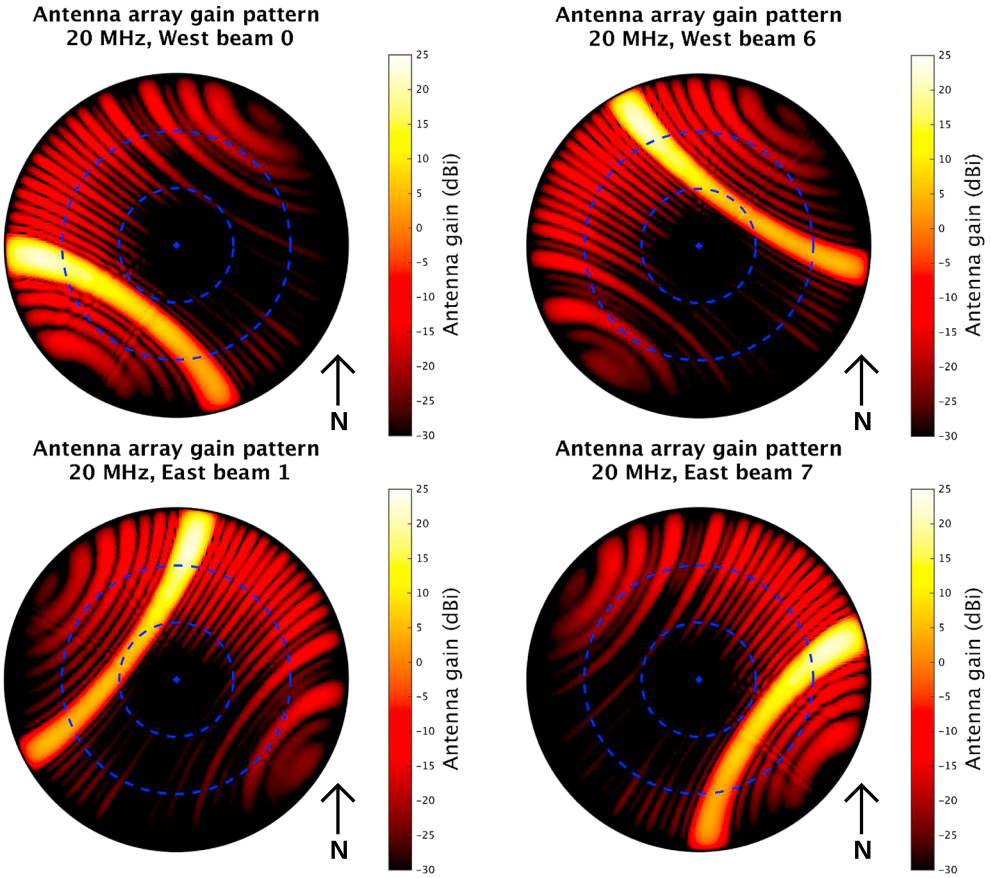

Figure 10. Antenna array gain patterns for the FMS array at JORN Laverton, for four different beams, at 20 MHz, calculated using NEC. The central point of each plot is the zenith, the outer boundary is the horizon and the two dashed circles represent 30° and 60° elevations. True north is at the top of the diagram.

information on the directional distribution of the noise, so it cannot be used to accurately estimate the background noise in this case.

Figures 9 and 10 show the antenna pattern for the FMS array at Laverton, calculated using NEC, for four different beam steer directions, at 10 MHz and 20 MHz. Note that the four beams are directed toward different noise environments: two beams are pointed toward the Indian and Pacific Oceans which both have very little lightning activity and thus a relatively low background noise, whereas the other two beams are directed northeast toward Southeast Asia, an area of frequent storms and thus a relatively high background noise (see the map in Figure 4; the four beams shown are the first, seventh, tenth, and sixteenth, counting clockwise from the westernmost beam).

Figure 11 shows the monthly median noise measured in these four beams for June 2012, compared to the results calculated by SPINE. The measurements are shown on the left with the modeled results on the right. SPINE is able to accurately represent the difference in background noise due to the different beam steer directions, as well as the overall diurnal and frequency variation of the noise. Additionally, SPINE can also predict the features shown at higher frequencies that are caused by relative movement of the galactic center; particularly striking is the short-term wideband increase caused by the galactic center crossing through the main lobe of the beam.

Note that SPINE is modeling the noise on a particular day (15 June), whereas the corresponding measurements are shown as a monthly median. As the galactic center's position in the sky will gradually shift over the course of the month, the monthly median data should show an increase that is smaller in magnitude but more spread in time compared to the model.

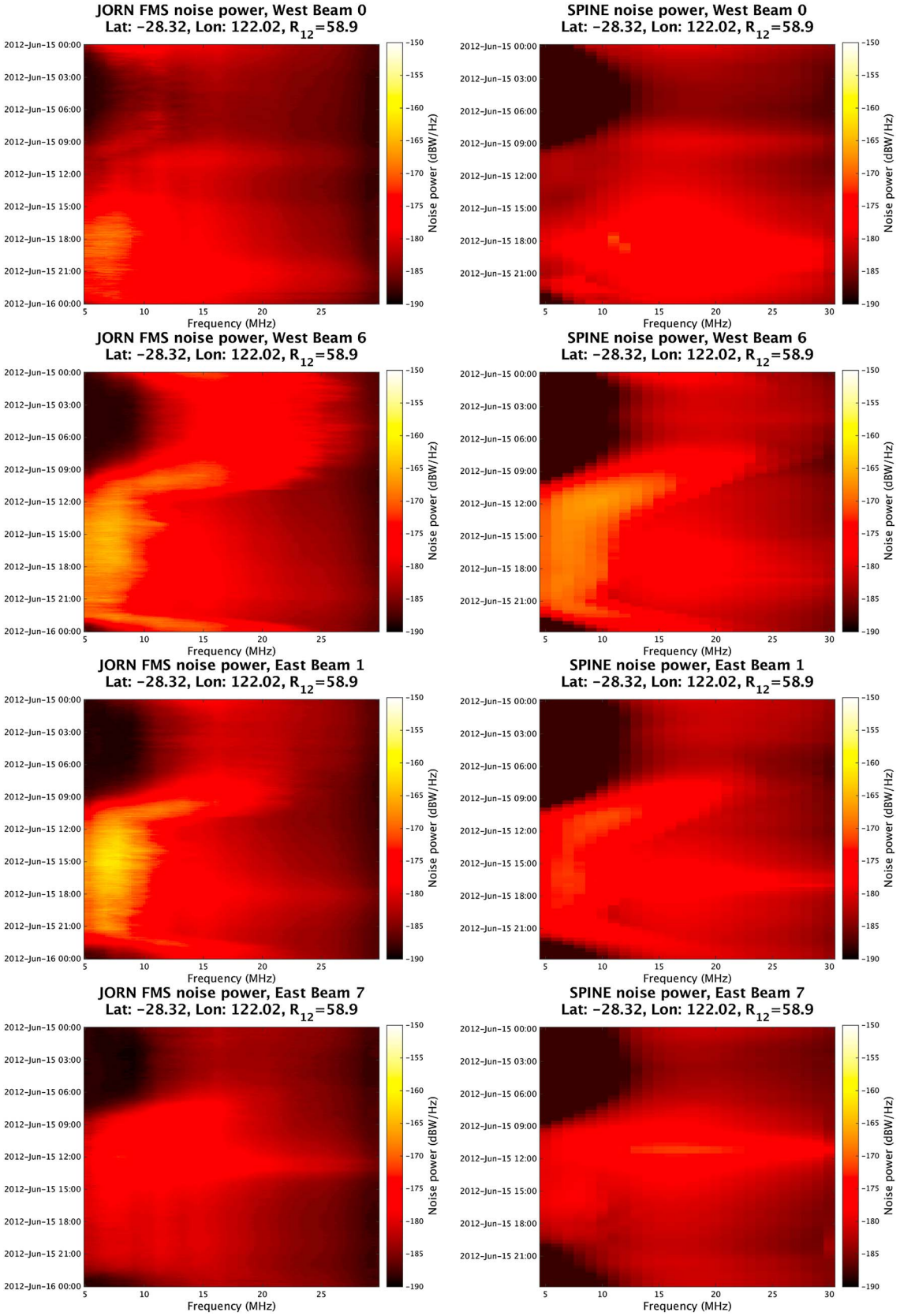

Figure 11. (left column) Monthly median noise measured by four different FMS beams at JORN Laverton during June 2012, (right column) compared to corresponding results simulated with SiMIAN.

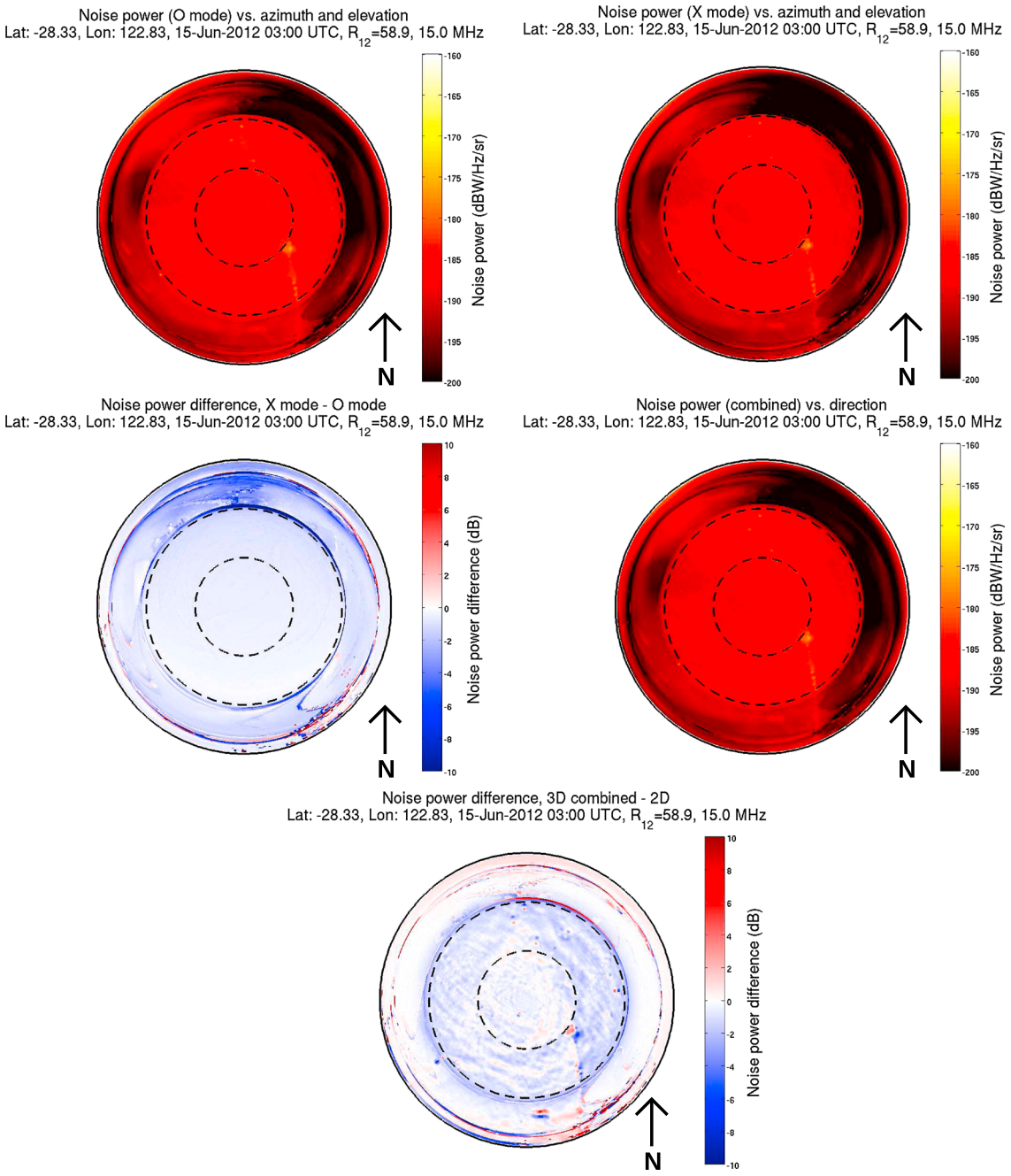

Figure 12. Directional noise power densities predicted by SPINE, using three-dimensional raytracing, at 15 MHz during daytime mid solar cycle conditions. Clockwise from top left: *O* mode, *X* mode, combined, the difference between the combined results and the 2-D results (from Figure 5) and the difference between the two modes.

6. Three-Dimensional Raytracing Results

While SPINE normally uses two-dimensional numerical raytracing for simplicity and speed, three-dimensional numerical raytracing (3-D NRT) can be used instead, which allows SPINE to include the effects of magneto-ionic splitting, although this requires much more time to calculate.

Figure 12 (top row) show results calculated using 3-D NRT, assuming that the noise sources radiate all of the power into one polarization (*O*-mode top left, *X*-mode top right). The center left panel shows the difference between the two modes. The *X*-mode has overall less power, due to greater absorption by the ionosphere. There is also a large difference between the modes at elevations where the propagation layer changes

(e.g., at approximately 45° where the propagation changes from *F* layer to transionospheric), as these occur at slightly different elevations for the different polarizations.

The center right panel shows the combined result, assuming that both the lightning and galactic noise sources radiate equal power into the *O* and *X* modes. This result is very similar to the 2-D NRT result shown in Figure 5 (bottom left panel) except for regions where the noise power drops sharply due to changes in the propagation path, e.g., at 10° elevation where the area of reduced power is wider and shallower (greater minimum power); the bottom panel shows the difference between the combined 3-D NRT result and the 2-D NRT result. The 3-D NRT result has approximately 1 dB less noise overall in this particular case. The differences are small enough that for most purposes the faster 2-D NRT model would be adequate.

7. Conclusion

This paper describes a model for natural environmental HF noise, which is based on the theoretical framework developed by *Coleman* [2002]. We have built upon in several areas, in particular a more accurate model for the absorption which is important for accurately predicting the noise at lower frequencies and the transionospheric propagation of galactic noise, as well as calibration against a 5 year data set of background noise measurements from JORN at Longreach. The model can predict the directional distribution of noise, as well as its diurnal, seasonal, solar cycle, and geographic variation. The model agrees well with measurements of noise from JORN at Laverton, matching the measurements much more closely than the standard ITU-R P.372 noise model.

The model has been developed for predicting the performance of HF systems, particularly systems using 2-D arrays. Knowing the directional distribution of noise, particularly the changes with elevation due to different propagation modes, is crucial for assessing the performance of new antenna array designs and ensuring the extra gain offered by them leads to increased sensitivity of the whole radar system.

Possible future enhancements to the model include further investigation and verification of the directional distribution of the background noise field, as well as the development of a model for man-made radio noise (i.e., the broadband radio emissions from devices such as vehicle ignition systems and power lines) which will improve the model's accuracy near urban areas.

Acknowledgments
The data from the JORN Frequency Management System used in this paper are from the Australian Department of Defence. Because of national security issues, the data cannot be released.

References

Bilitza, D., L. McKinnell, B. Reinisch, and T. Fuller-Rowell (2011), The international reference ionosphere today and in the future, *J. Geod.*, *85*(12), 909–920.

Burke, G. J. (1992), Numerical Electromagnetics Code—NEC-4, method of moments, Part I: User's manual and Part II: Program description—Theory, *Tech. Rep., UCRL-MA-109338*, Lawrence Livermore National Laboratory, Livermore, Calif.

Cecil, D. J., D. E. Buechler, and R. J. Blakeslee (2014), Gridded lightning climatology from TRMM-LIS and OTD: Dataset description, *Atmos. Res.*, *135*, 404–414.

Cervera, M. A., and T. J. Harris (2014), Modeling ionospheric disturbance features in quasi-vertically incident ionograms using 3-D magnetoionic raytracing and atmospheric gravity waves, *J. Geophys. Res. Space Physics*, *119*, 431–440, doi:10.1002/2013JA019247.

Coleman, C. J. (2002), A direction-sensitive model of atmospheric noise and its application to the analysis of HF receiving antennas, *Radio Sci.*, *37*(3), 1031, doi:10.1029/2000RS002567.

Cooray, V. (Ed.) (2003), *The Lightning Flash*, Energy Engineering, Institution of Engineering and Technology, Stevenage, U. K.

de Oliveira-Costa, A., M. Tegmark, B. Gaensler, J. Jonas, T. Landecker, and P. Reich (2008), A model of diffuse Galactic radio emission from 10 MHz to 100 GHz, *Mon. Not. R. Astron. Soc.*, *388*(1), 247–260.

Frazer, G., C. Williams, Y. Abramovich, and G. San-Antonio (2015), A regular two-dimensional over-sampled sparse receiving array for Over-The-Horizon Radar, in *Radar Conference (RadarCon)*, pp. 840–845, IEEE, Arlington, Va.

Giesbrecht, J., R. Clarke, and D. Abbott (2006), An empirical study of the probability density function of HF noise, *Fluctuation Noise Lett.*, *6*(02), L117–L125.

International Radio Consultative Committee (1964), *World Distribution and Characteristics of Atmospheric Radio Noise*, vol. *322*, International Telecommunication Union, Geneva, Switz.

International Telecommunication Union (2013), Recommendation ITU-R P.372-11: Radio noise, *Tech. Rep.*, International Telecommunication Union, Geneva, Switz.

Kotaki, M. (1984), Global distribution of atmospheric radio noise derived from thunderstorm activity, *J. Atmos. Terr. Phys.*, *46*(10), 867–877.

Lemmon, J. (1991), Model for the simulation of wideband HF noise and interference, in *Fifth International Conference on HF Radio Systems and Techniques*, pp. 349–353, IET, Edinburgh.

Lemmon, J. J. (2001), Wideband model of HF atmospheric radio noise, *Radio Sci.*, *36*(6), 1385–1391.

Lucas, D. L., and G. W. Haydon (1966), Predicting statistical performance indexes for high frequency ionospheric telecommunications systems, *Tech. Rep.*, DTIC Document, Boulder, Colo.

Northey, B. J., and P. S. Whitham (2000), A comparison of DSTO and DERA HF background noise measuring systems and the International Radio Consultative Committee (CCIR) model data, *Tech. Rep. DSTO-TR-0855*, Defence Science and Technnology Organisation, Edinburgh, Australia.

Pederick, L., and M. Cervera (2014), Semiempirical Model for Ionospheric Absorption based on the NRLMSISE-00 atmospheric model, *Radio Sci.*, *49*, 81–93, doi:10.1002/2013RS005274.

Picone, J. M., A. E. Hedin, D. P. Drob, and A. C. Aikin (2002), NRLMSISE-00 empirical model of the atmosphere: Statistical comparisons and scientific issues, *J. Geophys. Res.*, *107*, 1468, doi:10.1029/2002JA009430.

Rodriguez, S. P. (1997), High-frequency noise and spectrum occupancy measurements for Virginia and Texas with comparisons to International Radio Consultative Committee predictions, *Radio Sci.*, *32*(5), 2075–2082.

Sen, H. K., and A. A. Wyller (1960), On the generalization of the Appleton-Hartree magnetoionic formulas, *J. Geophys. Res.*, *65*, 3931–3950, doi:10.1029/JZ065i012p03931.

Shinde, M., and S. Gupta (1974), A model of HF impulsive atmospheric noise, *IEEE Trans. Electromagn. Compat.*, *EMC-16*(2), 71–75.

Ward, B., and M. Golley (1991), Solar cycle variations in atmospheric noise at HF, in *Fifth International Conference on HF Radio Systems and Techniques*, pp. 327–331, IET, Edinburgh.

Erratum

In the originally published version of this article, an author affiliation was omitted in error. The affiliation has been added and this version may be considered the authoritative version of record.